



Original Article

Interface monitoring of steel-concrete-steel sandwich structures using piezoelectric transducers

Jiachuan Yan ^{a, b, c}, Wensong Zhou ^{a, b, c, *}, Xin Zhang ^{a, b, c}, Youzhu Lin ^{a, b, c}^a Key Lab of Structures Dynamic Behavior and Control of the Ministry of Education, Harbin Institute of Technology, Harbin, 150090, China^b Key Lab of Smart Prevention and Mitigation of Civil Engineering Disasters of the Ministry of Industry and Information Technology, Harbin Institute of Technology, Harbin, 150090, China^c School of Civil Engineering, Harbin Institute of Technology, Harbin, 150090, China

ARTICLE INFO

Article history:

Received 11 November 2018

Received in revised form

10 January 2019

Accepted 21 January 2019

Available online 22 January 2019

Keywords:

Steel-concrete-steel sandwich structures

Bond-slip

Interface monitoring

Acoustic emission

Electromechanical impedance

ABSTRACT

Steel-concrete-steel (SCS) sandwich structures have important advantages over conventional concrete structures, however, bond-slip between the steel plate and concrete may lead to a loss of composite action, resulting in a reduction of stiffness and fatigue life of SCS sandwich structures. Due to the inaccessibility and invisibility of the interface, the interfacial performance monitoring and debonding detection using traditional measurement methods, such as relative displacement between the steel plate and core concrete, have proved challenging. In this work, two methods using piezoelectric transducers are proposed to detect the bond-slip between steel plate and core concrete during the test of the beam. The first one is acoustic emission (AE) method, which can detect the dynamic process of bond-slip. AE signals can be detected when initial micro cracks form and indicate the damage severity, types and locations. The second is electromechanical impedance (EMI) method, which can be used to evaluate the damage due to bond-slip through comparing with the reference data in static state, even if the bond-slip is invisible and suspends. In this work, the experiment is implemented to demonstrate the bond-slip monitoring using above methods. Experimental results and further analysis show the validity and unique advantage of the proposed methods.

© 2019 Korean Nuclear Society, Published by Elsevier Korea LLC. This is an open access article under the CC BY-NC-ND license (<http://creativecommons.org/licenses/by-nc-nd/4.0/>).

1. Introduction

Steel-concrete-steel (SCS) sandwich structure is a composite structure system, comprised two external steel plates, core materials, shear studs and cross ties. Shear studs and cross ties are used to strengthen the connection action between the steel plates and the core concrete, shown as in Fig. 1. SCS sandwich structures combine the advantages of steel structure and reinforced concrete such as high bearing capacity, high ductility and integrity. It has also exhibited superiorities in high resistances, crack control and enhancing the construction efficiency. Recent years, SCS sandwich structures become popular for their important advantages, therefore they are frequently used in the special structures, such as nuclear structures [1,2] tunnels [3], bridges [4], and Arctic offshore [5].

The concept of sandwich structures was proposed by Solomon [6] in 1976, which was used in large span bridges. Later Tomlinson [7] named double skin sandwich structure (DSC) to design the project of North Wales Conway tunnels, where headed studs were used as shear connectors. The development of Bi-steel system was an important process in SCS construction. Bowerman [8] presented the Bi-steel system, which used transverse short bars as mechanical shear connectors instead of headed studs. In recent years, researchers carried out a lot of works to study the structural behavior of SCS structural members. Wright [9] conducted 53 groups of steel plate-concrete beams tests to define the failure patterns of DSC structure, which took into account the effect of section depth, shear-span ratio, and shear reinforcement ratios on specimens. Wang [10] predicted the bending resistance of SCS sandwich structures through analyzing the mechanical responses of SCS sandwich panels. Leng [11] analyzed the mechanical properties of SCS beams. Yang [12] conducted a series of SCS sandwich wall tests to investigate the seismic behavior, which took the effect of local buckling of steel plate into consideration.

It is easy to understand that the advantages of SCS sandwich

* Corresponding author. Key Lab of Structures Dynamic Behavior and Control of the Ministry of Education, Harbin Institute of Technology, Harbin, 150090, China.
E-mail address: zhouwensong@hit.edu.cn (W. Zhou).

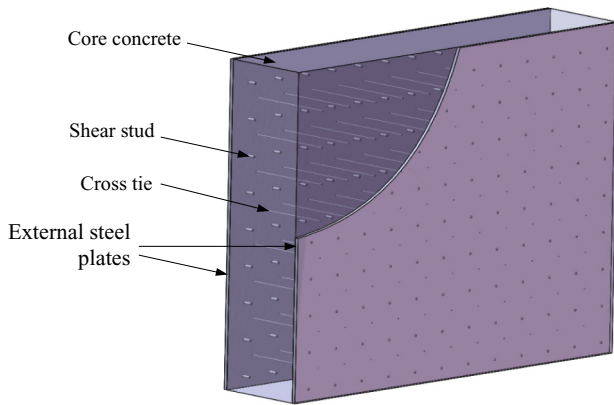


Fig. 1. Steel-concrete-steel sandwich structure.

structures are heavily dependent on the interface bonding quality between the steel plates and the core concrete. In case of severe bond-slip, SCS structures will lose their integrity, the bearing capacity and their fatigue life will be affected too. Therefore, bond-slip monitoring has attracted great attention from the research and engineering communities, especially the structural health monitoring and NDT communities. Interface monitoring is a common problem for various composite structures. Among all existing NDT techniques used to monitor interface bonding quality, ultrasound-based methods seem to be the most suitable methods because they interrogate the interface mechanically [13–17]. Guided ultrasonic waves, including Lamb wave and shear horizontal (SH) guided wave, are more suitable to the thin structures, such as metal plate and composite laminates. Guo and Cawley [18] studied the interaction of the S_0 Lamb mode with delamination in composite laminates both by finite element analysis and by experiment. It's shown that S_0 mode reflected from a delamination strongly. Seifried et al. [19] developed the analytical and computational models to quantify the propagation of Lamb waves in multi-layered, adhesive bonded components. Okabe et al. [20] applied the guided wave method on the fiber metal laminates, which consisting of FRP composites and thin metal foils. They used the mode conversion of Lamb waves to estimate the delamination quantitatively. Besides, SH waves were also employed to identify the adhesive properties at interfaces located within two metallic plates [21]. However, for the SCS sandwich structures, due to the existence of thick concrete the ultrasonic waves propagates with more complicated manners. For the interface detection between steel plate and concrete, several attempts have also been made to experimentally quantify the damage degree. Tsuyuki et al. [22] proposed a non-destructive testing method based on velocity dispersion analysis of laser ultrasonic waves for the delamination detection between the steel plate and the concrete. They simulated the delamination using a bolt penetrated through the steel of the specimen. Cheng et al. [23] studied the dispersive characteristics of the Lamb wave modes traveling within the steel layer to assess the bonding condition. The frequency-phase velocity images obtained from the numerical models were used to evaluate the bond condition. Qin et al. [24] developed another active sensing approach using smart aggregates to detect the initiation and to monitor the development of bond-slip between the steel plate and the concrete. The swept sine wave was generated and excited by the smart aggregates. The wavelet packet decomposition of the received stress wave signals from smart aggregates can evaluate the bond-slip quantitatively.

Most of above investigations based on ultrasound methods

employed the piezoelectric transducer pairs to excite and receive the stress waves. They can be considered as the active methods, and usually need the materials parameters and geometry information, such Young modulus, density and the thickness of the steel plate, as the priori knowledge to identify the damage. In addition, waveforms are difficult to interpret for such structures with complex formation by using ultrasound methods. In this work, by using less piezoelectric transducers, acoustic emission and electromechanical impedance methods were employed to monitor the interface between the steel plate and the concrete. The former is able to detect the stress waves emitted from the bond-slip passively and dynamically at very early stage when the microcracks form initially. Meanwhile, the displacement measurement between the steel plate and concrete has hardly response, and the changing strain doesn't have the direct relationship with the bond-slip. The latter can monitor the variations in structural mechanical impedance caused by the presence of bond-slip, even though the process of bond-slip stop or invisible. Both methods are robust and need less the priori knowledge. In practical applications, the acoustic emission and electromechanical impedance signals can be obtained using the same piezoelectric transducers attached permanently on the surface of or embedded within the SCS sandwich structures. In the remaining part of this paper, the physical principle of these two monitoring methods will be presented first. Then, the setup and procedure of the experiment on SCS sandwich beams under shear load will be described in detail. The results of structural tests and interface monitoring will be discussed finally.

2. Interface monitoring methods

2.1. Acoustic emission method

The most immediate physical phenomenon associated with structural failure, i.e. the splitting cracks, between the steel and the concrete is acoustic emission (AE), which can be detected by AE sensors, usually the piezoelectric transducers attached on the surface of materials or components and be presented as AE signals. They are elastic waves formed due to release of the elastic energy in the material, and accompany only active damages that are initiated

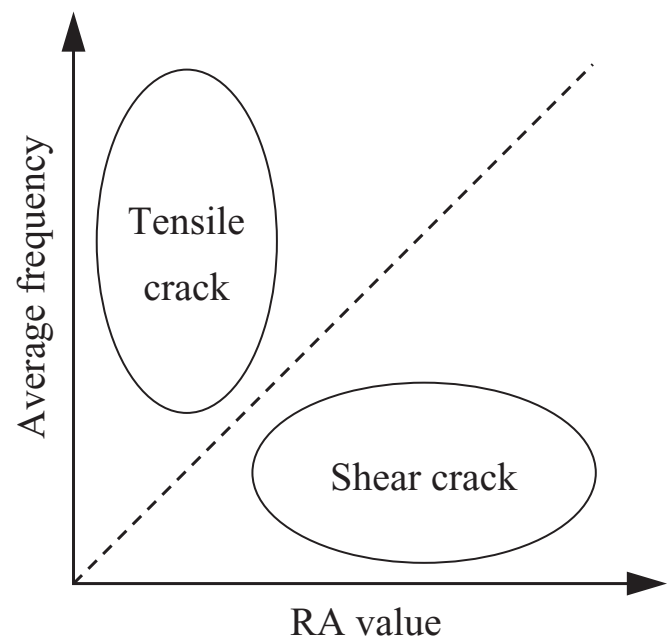


Fig. 2. Crack classification using AE signals characteristics.

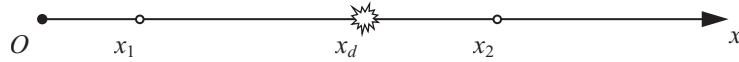


Fig. 3. Damage localization in the one-dimensional structure using AE signals.

$$x_d = \frac{x_1 + x_2 + \Delta t \cdot v}{2} \quad (3)$$

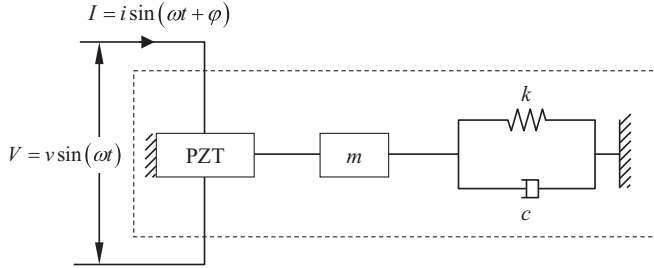


Fig. 4. The one-dimensional mechanical-electric coupling model of PZT-structure.

or developed during subjected loading conditions. AE signals monitoring is a unique, non-invasive and passive non-destructive testing method. By means of analyzing the classical characteristics of AE signals in time and frequency domains, such as amplitude, energy, average frequency, peak frequency, counts, rise time etc., the structural damages can be identified, localized, and quantified. Moreover, the classification of cracks using AE also has been explored [25,26]. There are many methods of crack classification have been utilized such as *b*-value [27–29], RA value, calm ratio etc.

The *b*-value is used frequently to evaluate the crack scale. It is derived from frequency-magnitude distribution data via the Gutenberg-Richter relationship used widely in seismology. In the AE signal analysis, the Gutenberg-Richter relationship is rewritten as [28]:

$$\log_{10} N = a - b \left(\frac{A}{20} \right) \quad (1)$$

where *N* is the number of AE events with amplitude greater than the threshold value; *A* is the peak amplitude of AE events; *a* is an empirical constant and *b* is the AE based *b*-value.

For AE applications, the *b*-value is defined as the log-linear slope of the frequency-magnitude distribution of AE signals. It can be used to evaluate the structure failure progression [27].

$$b = \frac{20 \log_{10} e}{\langle A \rangle - A_{\min}} \quad (2)$$

where $\langle A \rangle$ is the mean amplitude and A_{\min} is the threshold amplitude chosen for detecting the AE.

Moreover, from the view of crack modes, the tensile crack involves the opposing movement of the crack sides, which results in AE signals with short rise time and high frequency, while the AE signals generated from shear crack have low frequency and longer rise time. Based on above mechanism, the Japanese building code

(JCMS-III B5706) [30] proposed a methodology for the crack classification, in which the structural damages can be classified into tensile and shear modes by RA value and average frequency (AF). RA value is defined as the ratio of rise time by the amplitude, i.e. RA = rise time/peak amplitude, shown as Fig. 2. But a defined criterion on the proportion of AF and RA has not been established yet.

AE signals can be also used to locate the damage source. In this work, the SCS sandwich beam can be considered as the one-dimensional structure, in which the piezoelectric sensors and damage source are in a line. It has been proven that two sensors have to put on both sides of the damage source, shown as Fig. 3, so that the damage source can be located using Eq. (3). where x_1 , x_2 and x_d are the location of sensors and damage source, respectively. Δt is the arrival time difference between two sensors. *v* is the stress wave velocity on the surface of concrete, which is considered as the constant here and is estimated by pitch-catch method along the lengthwise direction before the test.

In this work, AE signals were collected during the whole loading procedure, and were analyzed adequately to evaluate the bonding state of the SCS sandwich beam.

2.2. Electromechanical impedance (EMI) method

EMI can be considered as the indirect parameter associated with bonding failure. Because bonding failure impairs the integrity of SCS sandwich structures, and causes direct changes in the structural stiffness and/or damping, and then the structural mechanical impedance. However, it is difficult to measure the structural mechanical impedance directly. The feasible approach is measuring the electrical impedance of piezoelectric transducers bonded on structures. Because of the electromechanical coupling effect of piezoelectric transducers, the obtained electrical impedance is directly related to the mechanical impedance. By comparing that to a baseline impedance measurement, the bonding failure can be determined qualitatively. When the piezoelectric wafer is bonded on the surface of the structures, the one-dimensional mechanical-electric coupling model can be described as Fig. 4 [31]. For this system, Liang et al. demonstrated that the admittance *Y*, which is

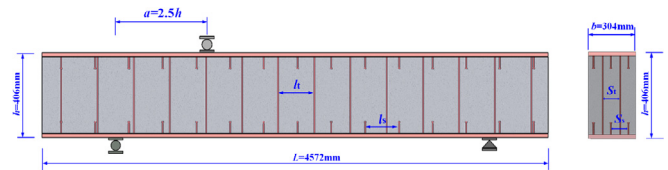


Fig. 5. Dimensions and fabrication details of specimen.

Table 1

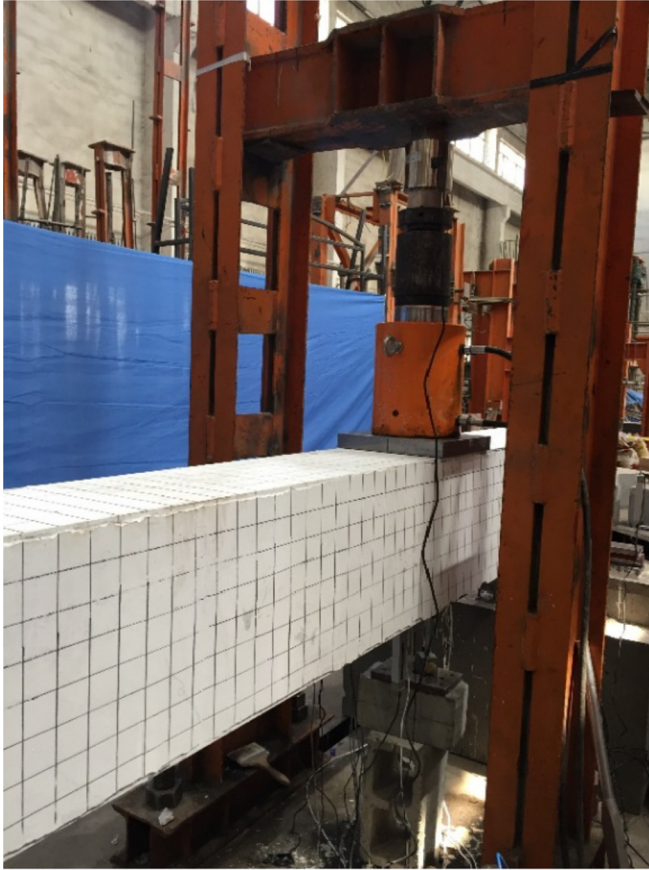
The geometric parameters and material properties of specimen.

Specimen	<i>a</i> (mm)	<i>f_c</i> (MPa)	<i>f_{y,tie}</i> (MPa)	<i>f_y</i> (MPa)	<i>d_{tie}</i> (mm)	<i>S_s</i> (mm)	<i>l_s</i> (mm)	<i>S_t</i> (mm)	<i>l_t</i> (mm)	$\rho_{t, \text{test}}$ (%)
SC1A	1015	107.8	435	373	8	152	220	102	203	0.163

Table 2

Mix proportions of UHPC (mass/cement mass ratio).

Water binder ratio	Cement	Silica fume	Superplasticizer	Quartz sand		Volume fraction of steel fibers
				Fine	Coarse	
0.2	1	0.25	0.02	0.61	0.49	2%

**Fig. 6.** The loading setup of tests.

the inverse of the impedance, of the piezoelectric transducer can be written as Eq. (4) [31].

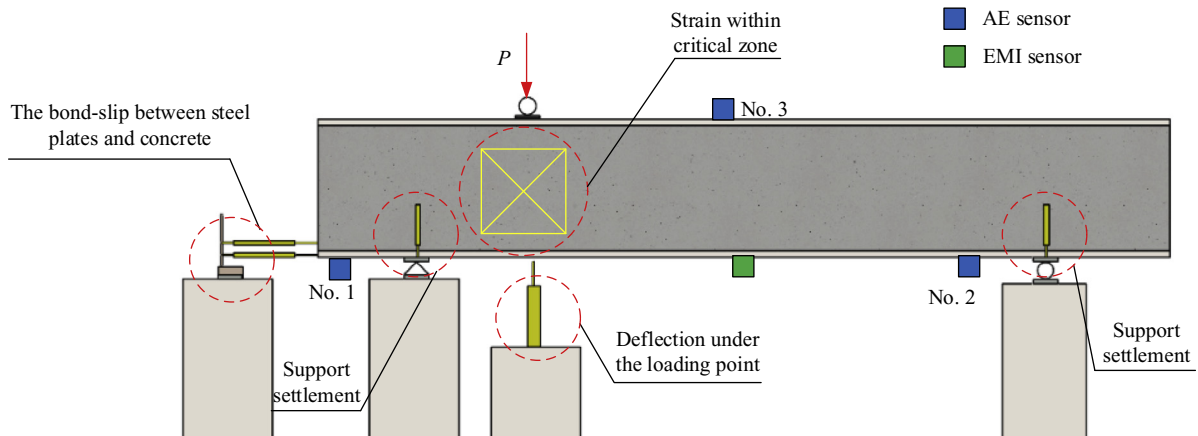
$$Y = i\omega \frac{b_p l_p}{h_p} \left(\bar{\epsilon}_{33}^T - \frac{Z}{Z + Z_A} d_{31}^2 \bar{E}_p \right) \quad (4)$$

where b_p , l_p and h_p are the dimensions of the piezoelectric transducer; Z and Z_A are the structure's and piezoelectric transducer's mechanical impedances, respectively; $\bar{\epsilon}_{33}^T$ is the dielectric constant at zero stress; d_{31} is the piezoelectric coefficient, and \bar{E}_p is the Young's modulus of the piezoelectric transducer. Since the electrical impedance signals collected by the sensor are the frequency-dependent for each structural state, the change of the impedance signal can be quantified by some damage metrics. Root mean square deviation (RMSD) is one of the most frequently used indices and defined as [32]:

$$RMSD(\%) = \sqrt{\frac{\sum_{i=1}^n [\text{Im}(Y_i) - \text{Im}(Y_i^0)]^2}{\sum_{i=1}^n [\text{Im}(Y_i^0)]^2}} \quad (5)$$

where $\text{Im}(Y_i)$ is the imaginary part of the measured admittance, i.e. the susceptance at the i th frequency value, and $\text{Im}(Y_i^0)$ is the susceptance measured at healthy conditions. Actually, the real part of the admittance is often used in some specific applications depending on their sensitivities to the damage.

Unlike the AE signals, EMI is an active sensing method, which can be implemented on the static structure, i.e. there are no active loading and active bonding failure in the meanwhile. In this work, EMI signals were collected when the loading suspends, and then were analyzed to evaluate the bonding state of the SCS sandwich beam.

**Fig. 7.** The details of the test design.

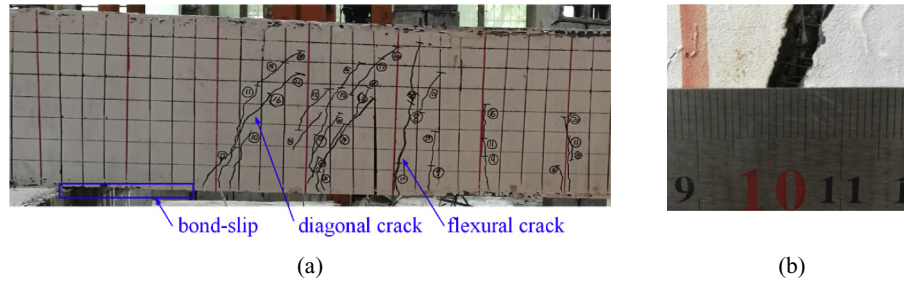


Fig. 8. The crack distribution for SCS sandwich specimen.

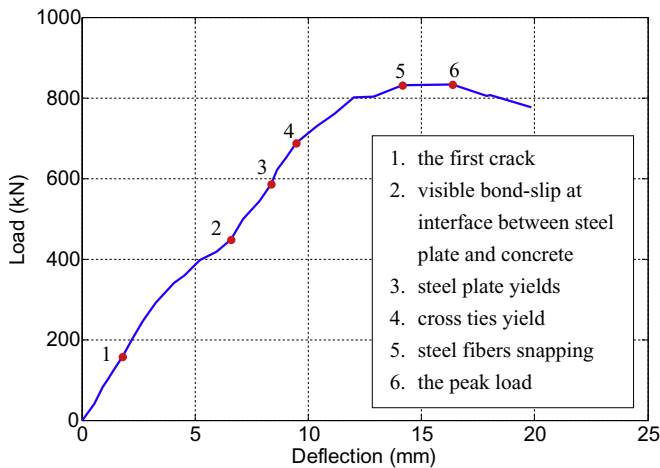


Fig. 9. The load-deflection curve of the specimen.

3. Experimental setup and procedure

The test of simply supported SCS sandwich beam was conducted under shear load. The dimensions of SCS sandwich beam was the depth of 406 mm, the length of 4572 mm and the width of 304 mm. Table 1 shows the fabrication details of geometric parameters and material properties. Dimensions and fabrication details were shown in Fig. 5. The shear span-to-depth ratio of SCS sandwich beam was designed identically with 2.5, which would be govern by

shear force according to Kani's Valley [33].

Note: a is the distance between the support and the loading point; f_c is the measured value of axial compressive strength for concrete; $f_{y, \text{tie}}$ is the measured value of yield strength of cross ties; f_y is the measured value of yield strength of steel plates; d_{tie} is the diameter of shear studs; S_s is the spacing of shear studs transversally, l_s is the spacing of shear studs longitudinally; S_t is the spacing of cross ties transversally; l_t is the spacing of cross ties longitudinally; $\rho_{t, \text{test}}$ is the shear reinforcement ratio of beam.

3.1. Core materials

Ultra-high performance concrete (UHPC) was adopted as the core materials for SCS sandwich beam. UHPC was made of ordinary Portland cement grade 42.5 (the minimum desired strength value achieved within 28 days), silica fume, quartz sand, water, super-plasticizer and steel fibers. The mix proportions were given in Table 2. During the casting of beam specimens, three prism specimens with the dimension of 100 mm × 100 mm × 400 mm were prepared to carry out the compression tests for obtaining the material properties of core concrete, as shown in Table 1. The testing machine satisfies the standard requirements in GB/T 2611–2007 [34], of which loading capacity is 1000 kN. The testing procedure is carried out according to GB50081-2002 [35].

3.2. Steel plates, shear studs and cross ties

Steel plates were adopted Q345 with the thickness of 9.8 mm. The tensile tests were conducted to obtain the material properties of steel plates, as shown in Table 1.

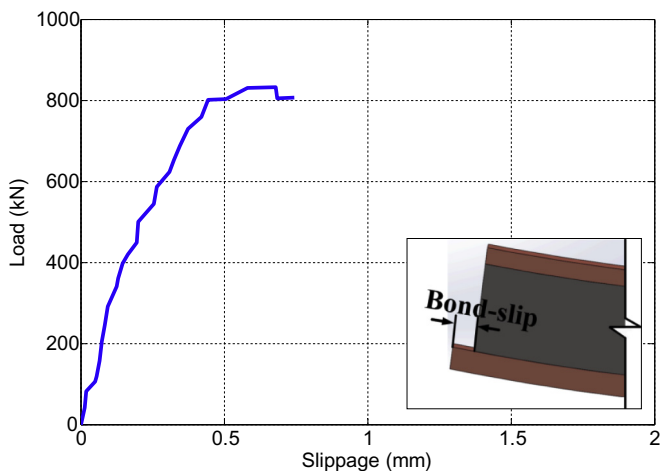


Fig. 10. The shear force-bond-slip curve of specimens.

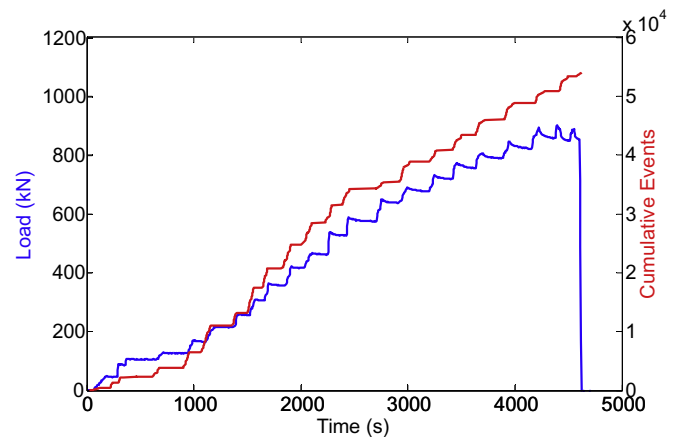
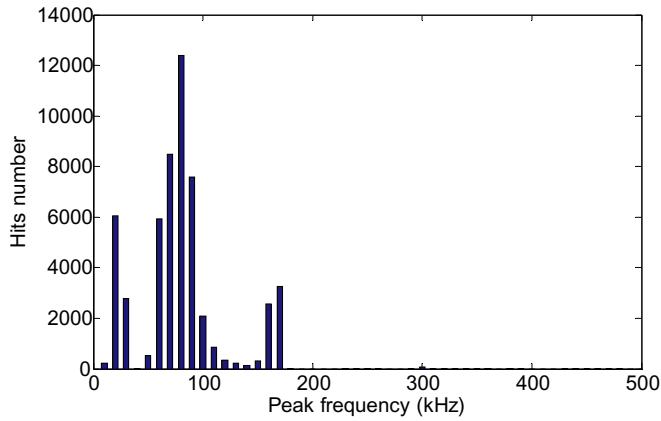
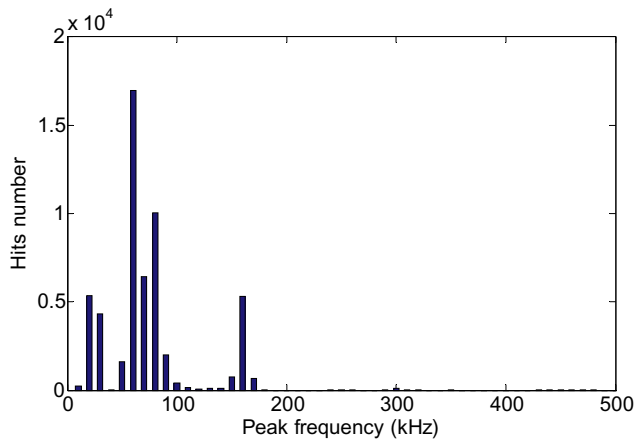


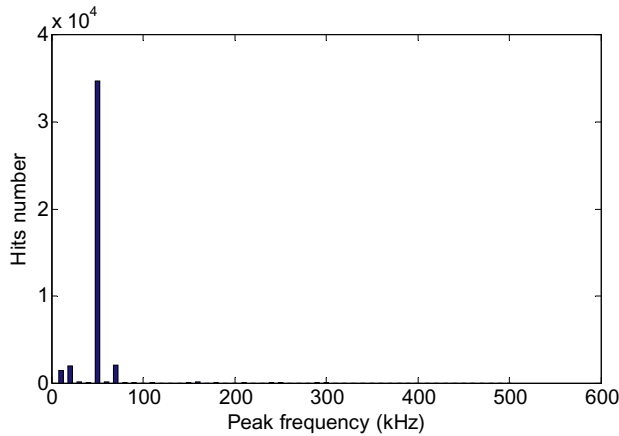
Fig. 11. History curves of the load with the cumulative events.



(a)



(b)



(c)

Fig. 12. Statistics distribution of the peak frequency: (a) sensor No. 1, (b) sensor No. 2, (c) sensor No. 3.

Shear studs were designed with the dimensions of the diameter 10 mm, length 80 mm and yield strength of shear studs 400 MPa respectively. And the spacing of shear studs was 220 mm longitudinally and 102 mm transversally.

Cross ties were designed according to the ACI349-06 Code [36]:

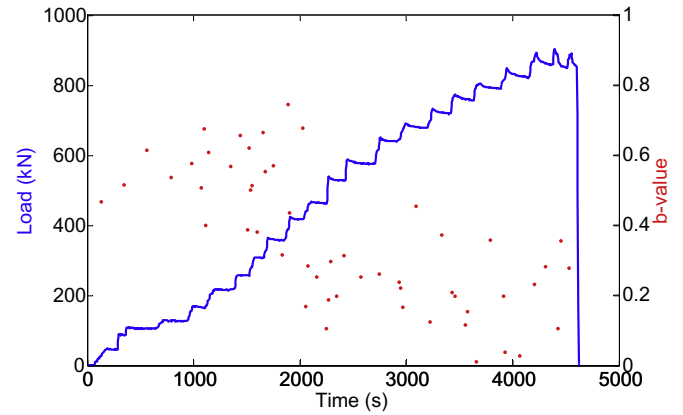


Fig. 13. b-value-load-time distribution.

$$\rho_{t,ACI} = 0.062 \frac{\sqrt{f_c}}{f_{y,tie}} \geq 0.35 \frac{1}{f_{y,tie}} \quad (6)$$

where, $\rho_{t,ACI}$ is the specified value of the shear reinforcement ratio. In terms of Eq. (6), the minimum reinforcement ratio was determined.

3.3. Experimental procedure and measuring scheme

The SCS sandwich beam was loading under three point loads, where the loading capacity of the testing machine was 2000 kN and the force controlled loading was through a lifting jack, as shown in Fig. 6. Fig. 7 shows the details of the test design as well as the all measurement systems. LVDTs were used to measure the vertical deflection under the loading point, and the bond-slip between steel plates and concrete horizontally. Strain gauges were set to measure the strains of cross ties and steel plates, as shown in Fig. 7. Below are brief summaries of the other two nondestructive testing systems, i.e. the AE system and the electrical impedance measurement system.

The AE system used in this work is DiSP-4/PCI system, product of Physical Acoustic Corporation, US. The digital bandpass filter is set between 10 kHz and 2 MHz, which covers the frequency range of the damage patterns of the SCS sandwich beam. The preamplifier has a gain of 40 dB, and the triggering threshold of data acquisition is 50 dB for rejecting the possible noise signals. Three AE sensors, model R15 α , were bonded on the surface of the beam, shown as Fig. 7. Two of them were placed on the both sides of the expectant bonding failure area under the beam to collect the AE signals. Thus, the data can be used to locate the bonding failure area. Another one was placed on the top side of the beam, which was used to collect the AE signals from concrete. The sampling rate for all sensors is 5 MHz.

The electrical impedance signatures were directly measured by the impedance analyzer (Agilent 4294A) over a given frequency range from 100 Hz to 900 kHz. One piezoelectric transducer was placed on steel plate on the underside of the beam, where is close to the possible bonding failure area.

4. Results and analysis

4.1. Failure pattern

For SCS sandwich beam, the failure pattern belongs to the flexural-shear failure with bond-slip characterized by the critical

flexural crack formed in shear span and the bond-slip at the interface between steel plate and concrete. As shown in Fig. 8(a), the flexural crack appeared in mid-span first and penetrated upward from the bottom steel plate. The bond-slip and separation between bottom steel plate and concrete appeared. Further, the web-shear crack formed in shear span, where two ends penetrated towards the support and the loading point. The bottom steel plate and cross ties across the web-shear crack yielded. Finally, the critical crack formed which was initially from the flexural crack and the specimens failed. Fig. 8(b) shows the width of critical crack under the peak load. It should be noted that there is no bond-slip between top steel plate and concrete.

4.2. Load-deflection curve

Fig. 9 shows the load-deflection curve of the specimen. The vertical and horizontal axes are the load and the deflection below the loading point, respectively. As shown in Fig. 9, the SCS sandwich beam initially behaved linearly up to the appearance of first crack. The stiffness of the SCS sandwich beam decreased, which may be because the height of the compressive zone decreased by the cracks. However, the curve behaved linearly until the appearance of cracks between steel plate and concrete. Further, the stiffness of the beam reduced obviously due to the yielding of steel plates and cross ties. The curve increased nonlinearly up to the appearance of the critical crack, and the loading reached the peak load. After reaching the peak load, the curve sustained a short platform and decrease rapidly, which exhibited a little ductility of this failure pattern.

4.3. Bond-slip between steel plate and concrete

The bond-slip failure was a shear failure between steel plate and concrete, which had contribution to the failure of SCS sandwich beam. Fig. 10 shows the values of bond-slip between steel plate and concrete for the specimen measured by traditional measurement method, which indicated that even through the visible bond-slip at the interface between steel and concrete occurred, the relative displacement between the steel plate and core concrete was not obvious and the bond-slip was not avoided in SCS sandwich beam.

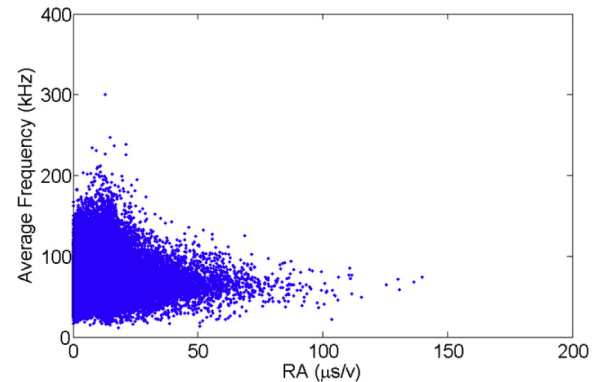
4.4. AE signals analysis

Although Fig. 9 shows the continuous loading curve, actually the loading was applied on the beam step by step. The loading process was divided into total 19 steps, which was shown as the blue curve in Fig. 11. The cumulative AE events from sensor No. 1 along with the loading process were shown as the red curve in this figure. It indicates that the cumulative AE events increase slowly at the beginning of loading process, which corresponds to the initial concrete cracks, and increase quickly after about 2000 s as well as the 400 kN load, when the failure of main structure occurred. This is the global feature of AE signals.

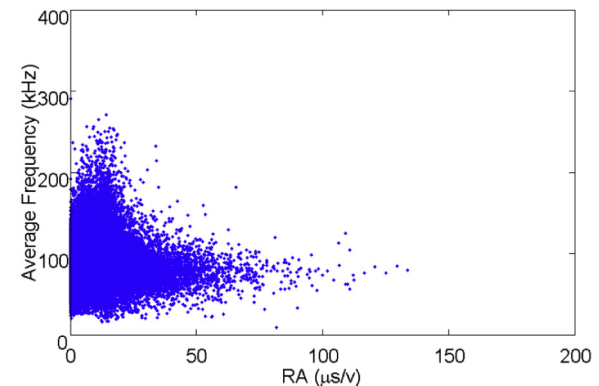
Fig. 12 shows the histogram of AE peak frequencies for three AE sensors, respectively. The two sensors attached on the bottom steel plate of the beam have the similar peak frequency distribution. The main frequency range is between 50 and 100 kHz, and even beyond 150 kHz. While the main frequency for the AE sensor No. 3, which was attached on the top of the beam is about 50 kHz. It is well known that due to the action of headed studs and cross ties, the shear strength between the steel and concrete is much larger than that of concrete, therefore the AE signals recorded by sensor No. 3 come from the concrete crack mainly, since there is no bond-slip between the top steel plate and concrete, while the sensors below collected mostly the AE signals from the bond-slip and the flexible cracks close to the steel plate.

Fig. 13 shows the b -value changed in response to time and load. Normally, the larger b -value indicates the micro-cracks begin to form, while the decreasing b -value indicates the macro-cracks are developing from micro-cracks. It can be found that the critical damage happened about 2000 s after loading. This loading step is identical to Fig. 11.

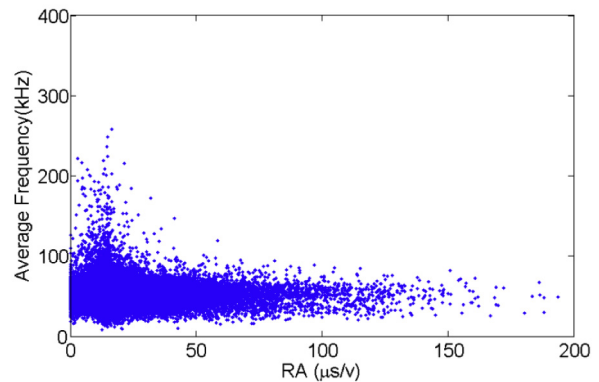
Since the failure pattern can be understood for the SCS sandwich beam tested in this study during the whole loading procedure, the relationship between AF and RA values from AE parameters is plotted for verifying the crack classification. Fig. 14 shows the RA and AF correlation distribution for all AE sensors. For the first two



(a)



(b)



(c)

Fig. 14. RA-AF correlation distribution: (a) sensor No. 1, (b) sensor No. 2, (c) sensor No. 3.

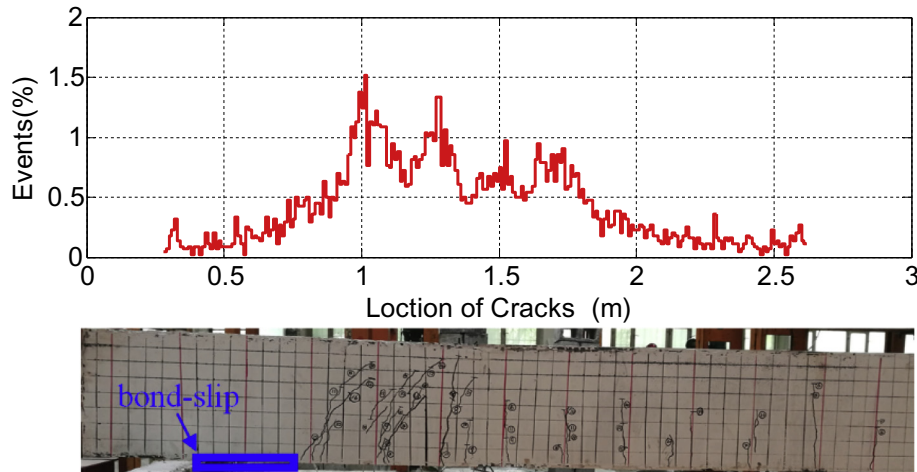


Fig. 15. Cracks localization using AE signals.

sensors under the beam, similar crack characteristics appear. The tensile, shear, and mixed cracks indicated in Fig. 14(a) and (b) were caused by the flexural crack of concrete in mid-span, the web-shear crack of concrete in shear span and bond-slip and separation between bottom steel plate and concrete, respectively, described as subsection 4.1. Fig. 14(c) indicates that the preponderant fracture mode is shear crack for the concrete, because the AE sensor at the top of the beam received hardly the signals produced in the lower part of the beam through the thick concrete.

Fig. 15 shows that results of cracks localization using the two AE sensors under the beam. It can be found that most of cracks located on the middle of the SCS sandwich beam. In the bond-slip area marked by the blue frame in Fig. 15, there are no visible cracks, therefore this small number of AE events corresponds to the bond-slip mainly. This illustrates in case the conventional measurement is difficult to be implemented, AE method can still detect the bond-slip.

4.5. EMI results analysis

The electrical impedance signals were collected by the piezoelectric transducer when the loading suspended for each loading level. Fig. 16 shows the susceptance vs. frequency curves at different frequency ranges for four representative loading levels. The susceptance is the imaginary component of the admittance, which is the reciprocal of impedance. The black curve is the baseline obtained when the structure has not been loaded yet. From Fig. 16(a), the lowest frequency range, for the first two loading levels, the curves don't change significantly, but for the last loading level corresponding to the later loading stage, when the beam has been damaged too much, the susceptance curve changes significantly. So, the susceptance is not sensitive for the early loading stages at this frequency range, but sensitive for the later loading stage, shown as the red curve in Fig. 16(a). Next frequency ranges, the susceptance signals have higher sensitivity increasingly for the early loading stages, while they have the similar sensitivity to all loading stages at the high frequency range, shown as Fig. 16(g)-(h). The susceptance signals shown in Fig. 16 indicate that the proposed method is able to estimate the structural failure.

The RMSD indices are calculated for low and high frequency

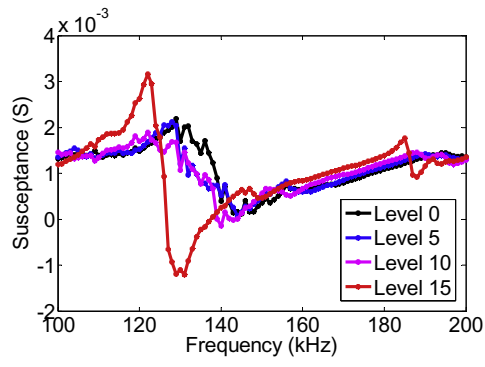
ranges, respectively, shown in Fig. 17. Both figures show that RMSD indices increase greatly at around loading level 10, which accords with the experimental phenomena. It can be found that the variation of RMSD index for the high frequency interval is more obvious with increasing the loading levels. However, all RMSD indices can indicate effectively the structural states induced the increasing loading.

5. Conclusions

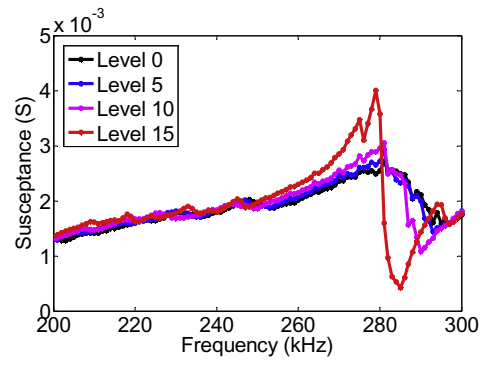
In this study, a SCS sandwich beam with shear connectors was designed and fabricated. It was tested under three point loads with the simply supported. The whole loading process was characterized by the load-deflection curve, in which the clear mechanical behavior can be distinguished. The failure pattern of the tested beam is the flexural-shear failure with bond-slip characterized by the critical flexural crack formed in shear span and the bond-slip at the interface between steel plate and concrete. Besides the conventional displacement measurement methods, the piezoelectric transducers were used to monitor the failure procedure of the SCS sandwich beam. Depending on two kinds of system, AE signals and EMI signals were collected during the step-by-step loading process, and used to evaluate the structural and bonding state.

The force, deflection and slippage data showed the change of conventional mechanical parameters, but they are difficult to describe the whole bonding failure, especially the initial stage. Results from AE sensors, which are close to the bonding area, can obtain more information about the bonding failure. AE signals can be recognized as the diagonal cracking and bonding failure according to their frequency characteristics firstly. Then the cracking process, mode and location can be identified using the AE signals. At the static state of the structure, the structural damage can be evaluated by using EMI signals, which reflect the local structural stiffness. Results indicates that RMSD index can describe the structural damage and are more sensitive at high frequency ranges.

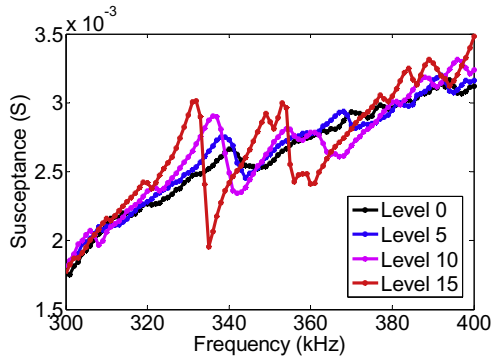
In practical applications, the AE and EMI signals can be obtained using the same piezoelectric transducers attached permanently on the surface of or embedded within the SCS sandwich structures, for the structural damage evaluation for different purposes.



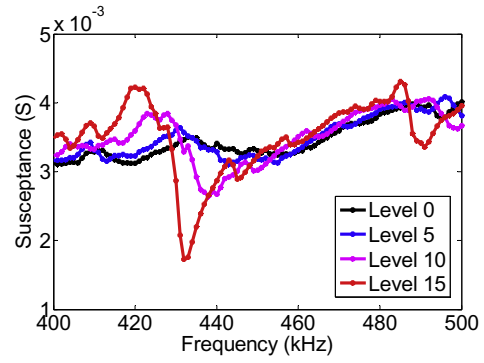
(a)



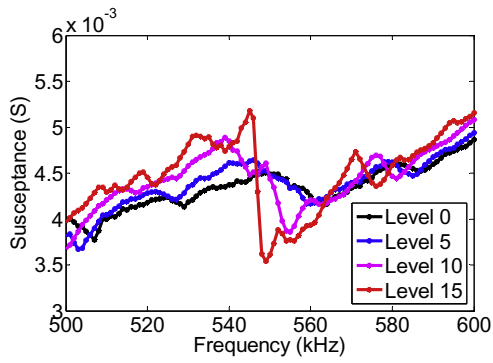
(b)



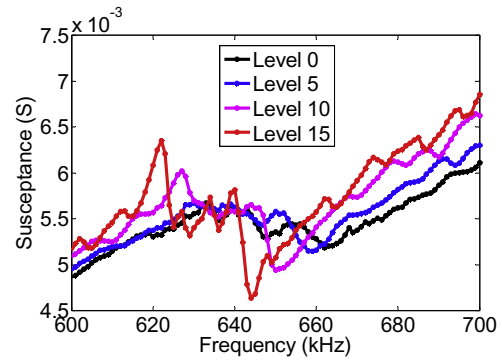
(c)



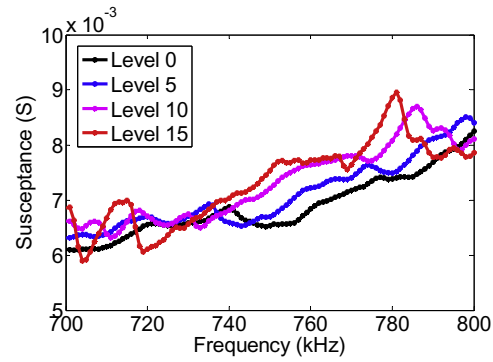
(d)



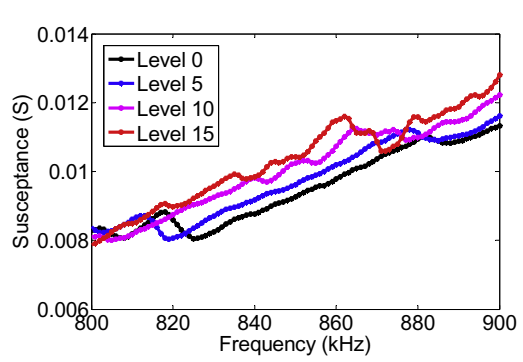
(e)



(f)



(g)



(h)

Fig. 16. The typical EMI curves for different loading level.

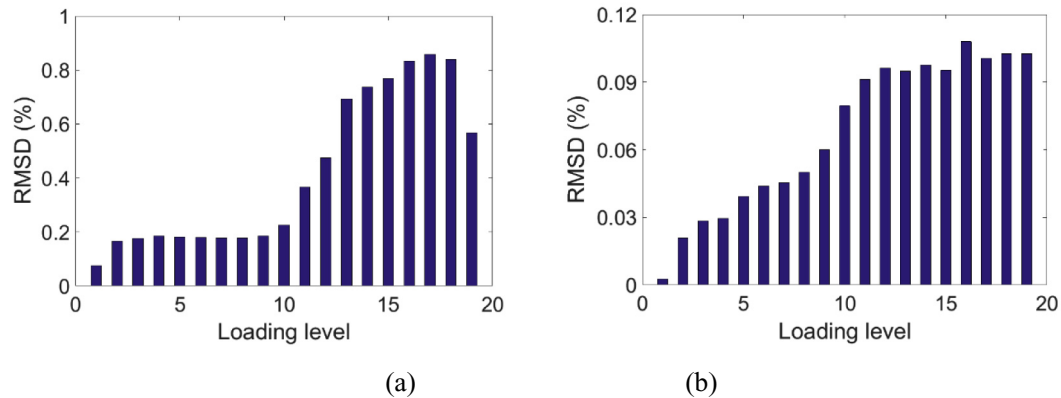


Fig. 17. RMSD value for all loading levels at two different frequency ranges: (a) 100–200 kHz, (b) 700–800 kHz.

Acknowledgements

The financial support from the National Key Research and Development Program of China under Grant Nos. 2018YFC1505304 and 2017YFC0703804; National Science Foundation of China under Grant Nos. 51578191 and 51308155 are appreciated gratefully.

References

- [1] T. Yamamoto, A. Katoh, Y. Chikazawa, K. Negishi, Design evaluation method of steel-plate reinforced concrete structure containment vessel for Sodium-Cooled fast reactor, *J. Disaster Res.* 7 (5) (2012) 645–655.
- [2] F. Qin, S. Tan, J. Yan, M. Li, Y.L. Mo, F. Fan, Minimum shear reinforcement ratio of steel plate concrete beams, *Mater. Struct.* 49 (9) (2015) 1–18.
- [3] J.W. Pryer, H.G. Bowerman, The development and use of British steel bi-steel, *J. Constr. Steel Res.* 46 (1) (1998), 15–15.
- [4] S. El-Bahey, M. Bruneau, Bridge piers with structural fuses and Bi-steel columns. I: experimental testing, *J. Bridge Eng.* 12 (1) (2012) 25–35.
- [5] J.B. Yan, J.Y.R. Liew, X. Qian, J.Y. Wang, Ultimate strength behavior of curved steel-concrete-steel sandwich composite beams, *J. Constr. Steel Res.* 115 (2015) 316–328.
- [6] S.K. Solomon, D.W. Smith, A.R. Cusens, Flexural tests of steel–concrete–steel sandwiches, *Mag. Concr. Res.* 28 (94) (1976) 13–20.
- [7] M.J. Tomlinson, A. Tomlinson, M.L. Chapman, et al., 17. Shell Composite Construction for Shallow Draft Immersed Tube Tunnels, *Immersed Tunnel Techniques*, 1990.
- [8] H. Bowerman, N. Coyle, J.C. Chapman, An innovative steel/concrete construction system, *Struct. Eng.* 80 (20) (2002) 33–38.
- [9] H.D. Wright, T.O.S. Oduyemi, H.R. Evans, The experimental behaviour of double skin composite elements, *J. Constr. Steel Res.* 19 (2) (1991) 97–110.
- [10] Y. Wang, J.Y.R. Liew, S.C. Lee, Ultimate strength of steel–concrete–steel sandwich panels under lateral pressure loading, *Eng. Struct.* 115 (2016) 96–106.
- [11] Y.B. Leng, X.B. Song, Experimental study on shear performance of steel–concrete–steel sandwich beams, *J. Constr. Steel Res.* 120 (2016) 52–61.
- [12] Y. Yang, J. Liu, X. Nie, J. Fan, Experimental research on out-of-plane cyclic behavior of steel-plate composite walls, *J. Earthquake Tsunami* 10 (01) (2016) 1650001.
- [13] M.N. Babu, C.K. Mukhopadhyay, G. Sasikala, S.K. Albert, A.K. Bhaduri, T. Jayakumar, R. Kumar, Study of fatigue crack growth in RAFM steel using acoustic emission technique, *J. Constr. Steel Res.* 126 (2016) 107–116.
- [14] M.G. Droubi, N.H. Faisal, F. Orr, J.A. Steel, M. El-Shaib, Acoustic emission method for defect detection and identification in carbon steel welded joints, *J. Constr. Steel Res.* 134 (2017) 28–37.
- [15] Y. Zhou, M. Dawood, B. Gencturk, High-cycle fatigue performance of high-mast illumination pole bases with pre-existing cracks, *J. Constr. Steel Res.* 138 (2017) 463–472.
- [16] T. Liu, D. Zou, C. Du, Y. Wang, Influence of axial loads on the health monitoring of concrete structures using embedded piezoelectric transducers, *Struct. Health Monit.* 2 (16) (2017) 202–214.
- [17] T. Liu, Y. Huang, D. Zou, J. Teng, B. Li, Exploratory study on water seepage monitoring of concrete structures using piezoceramic based smart aggregates, *Smart Mater. Struct.* 6 (22) (2013) 065002.
- [18] N. Guo, P. Cawley, The interaction of Lamb waves with delaminations in composite laminates, *J. Acoust. Soc. Am.* 94 (4) (1993) 2240–2246.
- [19] R. Seifried, L.J. Jacobs, J. Qu, Propagation of guided waves in adhesive bonded components, *NDT&E International* 35 (2002) 317–328.
- [20] Y. Okabe, H. Hirakawa, H. Nakatani, S. Ogihara, Delamination detection in fiber metal laminates using the mode conversion of Lamb waves, in: 7th European Workshop on Structural Health Monitoring, July 8–11, 2014, Nantes, France.
- [21] M.S.H. Castaings, Ultrasonic guided waves for the evaluation of interfacial adhesion, *Ultrasonics* 54 (2014) 1760–1775.
- [22] K. Tsuyuki, R. Katamura, S. Miura, H. Asanuma, Nondestructive Testing of Concrete Based on Analysis of Velocity Dispersion of Laser Ultrasonics, *European Conference on Non-Destructive Testing*, 2006.
- [23] C.C. Cheng, Y.T. Ke, K.T. Hsu, Using Lamb waves to evaluate debonding of steel plate strengthened concrete, *Mater. Trans.* 53 (2) (2012) 274–278.
- [24] F. Qin, Q. Kong, M. Li, Y. Mo, G. Song, F. Fan, Bond slip detection of steel plate and concrete beams using smart aggregates, *Smart Mater. Struct.* 24 (2015) 115039.
- [25] D.G. Aggelis, Classification of cracking mode in concrete by acoustic emission parameters, *Mech. Res. Commun.* 28 (2011) 153–157.
- [26] N.M. Nor, A. Ibrahim, N.M. Bunnori, H.M. Saman, Acoustic emission signal for fatigue crack classification on reinforced concrete beam, *Constr. Build. Mater.* 49 (2013) 583–590.
- [27] R.V. Sagar, B.K.R. Prasad, S.S. Kumar, An experimental study on cracking evolution in concrete and cement mortar by the b-value analysis of acoustic emission technique, *Cement Concr. Res.* 42 (2012) 1094–1104.
- [28] R.V. Sagar, M.V.M.S. Rao, An experimental study on loading rate effect on acoustic emission based b-values related to reinforced concrete fracture, *Constr. Build. Mater.* 70 (2014) 460–472.
- [29] P. Datt, J.C. Kapil, A. Kumar, Acoustic emission characteristics and b-value estimate in relation to waveform analysis for damage response of snow, *Cold Reg. Sci. Technol.* 119 (2015) 170–182.
- [30] Federation of Construction Material Industries, Monitoring Method for Active Cracks in Concrete by Acoustic Emission, *JCMS-III B5706*, Japan, 2003.
- [31] C. Liang, F.P. Sun, C.A. Rogers, Coupled electro-mechanical analysis of adaptive material systems – determination of the actuator power consumption and system energy transfer, *J. Intell. Mater. Syst. Struct.* 5 (1) (1994) 12–20.
- [32] F.P. Sun, Z. Chaudhry, C. Liang, C.A. Rogers, Truss structure integrity identification using PZT sensor-actuator, *J. Intell. Mater. Syst. Struct.* 6 (1) (1995) 134–139.
- [33] Kani GNJ, The riddle of shear failure and its solution, *ACI Struct. J.* 61 (4) (1964) 441–467.
- [34] GB/T 2611-2007, General Requirements for Testing Machines, China national standardization management committee, 2007.
- [35] GB50081-2002, Standard for Test Method of Mechanical Properties on Ordinary Concrete, The ministry of construction of China, 2002.
- [36] ACI 349M-06, Code Requirements for Nuclear Safety-Related Concrete Structures and Commentary (Metric), American Concrete Institute, Farmington Hills, 2006.